A 2-D UNSTEADY NAVIER-STOKES SOLUTION METHOD WITH OVERLAPPING/OVERSET MOVING GRIDS

Ismail H. Tuncer*
Department of Aeronautics and Astronautics
Naval Postgraduate School, Monterey, California
Phone: 408/656-2854, Fax: 408/656-2313
tuncer@aa.nps.navy.mil, http://www.aa.nps.navy.mil/~tuncer

ABSTRACT

A simple, robust numerical algorithm to localize intergrid boundary points and to interpolate unsteady solution variables across 2-D, overset/overlapping, structured computational grids is presented. Overset/overlapping grids are allowed to move in time relative to each other. The intergrid boundary points are localized in terms of three grid points on the donor grid by a directional search algorithm. The final parameters of the search algorithm give the interpolation weights at the interpolation point. The method is independent of numerical solution algorithms and it may easily be implemented on any 2-D, single block flow solver to make it a multi-block, zonal solver with arbitrarily overset/overlapping computational grids.

In the present study, numerical results are presented for steady and unsteady, viscous flow solutions over a flapping/stationary airfoil combination in tandem and over a single airfoil undergoing a sinusoidal flapping motion. The computational domains are discretized with overlapping and/or overset subgrids, which move in time relative to each other. The intergrid boundary point localization on the donor grid and the interpolation of flow variables are found to be accurate and robust. Computed flow variables are continuous across the grid boundaries and an excellent agreement is obtained against the single grid solutions.

INTRODUCTION

Among structured, block-structures and unstructured computational grids, structured grids still remain the most common in the CFD community.[1] The basic advantage of the structured grids is that they are still the most suitable for the highly efficient solution algorithms developed and refined since the early establishment of the science of CFD. Due to the inherent connectivity information, numerical solution algorithms with structured grids are easy to implement on conventional, shared memory/multi–processor computers.

In discretizing complex geometries and irregular boundaries, the block–structured grid techniques[2,3], where a group of structured grid blocks are patched together with enforced continuity across the interfaces, are currently being utilized. Although the block-structured grids have all the inherent advantages of structured grids, they are not well suited for unsteady flow problems with moving boundaries, in which all the grid blocks need to be regenerated at every time step in order to satisfy the continuity across interfaces.

The recent applications of unstructured grids[1,4] offer a promising alternative for treating irregular boundaries. However, for computation of unsteady flows with moving boundaries, the whole computational grid has to be regenerated at every time step similar to the block–structured grids. This process may become quite complex and costly[6]. Furthermore, the application of algebraic turbulence models in viscous flow problems, which utilizes the direction normal to solid surfaces, causes additional difficulties in unstructured grid topologies.[4,5]

An alternative for treating complex geometries with moving boundaries is the use of overset grids, in which individual structured grids are overset on each other and free to move with respect to each other. In the present work, a new method is presented for the solution of the unsteady Navier-Stokes equations on overlapping/overset structured grids, which are allowed to move relative to each other. The present method is similar to the Chimera/Pegsus[7] approach in essence. However, the two approaches differ in the way the over-

*Research Assistant Professor, member AIAA lapping boundaries are localized and the flow variables are interpolated.

In Pegsus, the localization of boundary points and the interpolation of flow variables across grid boundaries are done in several stages. First, all the grid points on the base grid are tested to determine if they lie within a certain distance from a temporary origin placed in the overlapping grid. All the grid points within the specified distance are next tested once more to see if they lie inside or outside of the overlapping grid boundary. The sign of the vector $\vec{N} \cdot \vec{R}$, where $\vec{R}$ is the relative position vector of the grid points and $\vec{N}$ is the unit outward normal at the cross-section of $\vec{R}$ and the overset grid boundary, determines the right direction. The closest points outside of the overlapping boundary are then assigned as the boundary points on the base grid. Finally, interpolation cells on the base grid, into which a boundary point of the overlapping grid falls, are localized, and the corresponding bilinear interpolation data are stored in an external file to be utilized by the flow solver. For unsteady flows, the Pegsus code has to be integrated into the flow solver and to be executed at every time step.

In the present work, the boundary point localization and interpolation of flow variables are integrated into a directional search algorithm in the main flow solver. The directional search algorithm localizes the boundary points sequentially and no external data is stored. Thus, the application of overlapping/overset grid boundary conditions is quite robust and efficient.

BOUNDARY POINT LOCALIZATION

In the present approach, the intergrid boundary points on overset/overlapping subgrids are localized on the adjacent/donor grids with a directional search algorithm. The directional search algorithm is depicted in Figure 1. Here, a single point, P, denoted by the + sign, is localized on a Cartesian grid in terms of the three closest grid points, which constitute a triangle. The search process starts from an arbitrary grid point $G_{i,j}$ as denoted in the figure. It is then tested to see if the point P falls into the triangle defined by grid points at $G_{i,j}, G_{i\pm1,j}$ and $G_{i,j\pm1}$, where the correct sign $\pm$ is determined by the search direction. The search direction is based on the geometry gradients on the grid. The test whether the point P falls into the triangle is based on the representation of a convex surface defined by three points and determined by the solution of the following three linear equations in terms of α, β and γ. Since, any point in a convex triangular surface may

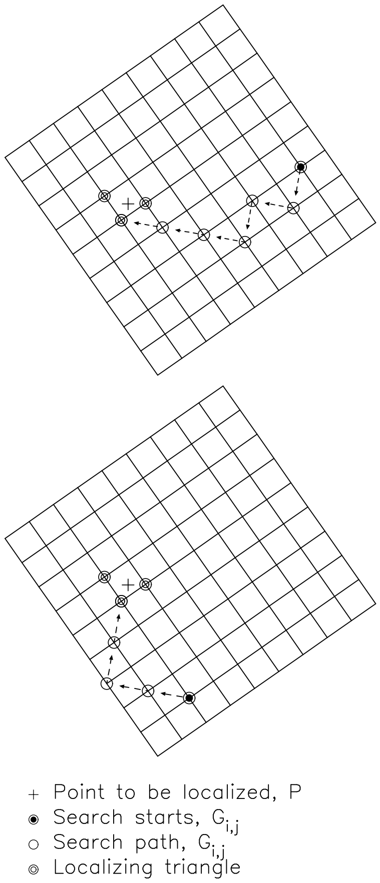

Fig. 1a Localization of a point

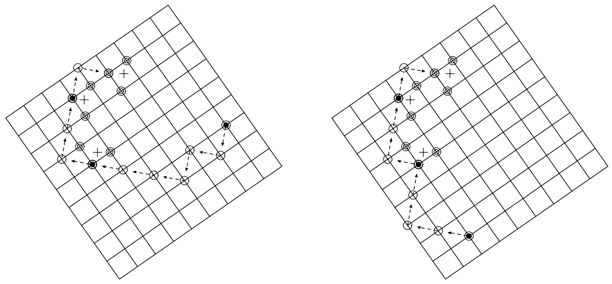

Fig. 1b Sequential localization of points

uniquely be represented by three real numbers provided that they are all positive.

$$\begin{aligned} X_P &= \alpha\, X_{i,j} + \beta\, X_{i\pm1,j} + \gamma\, X_{i,j\pm1} \\ Y_P &= \alpha\, Y_{i,j} + \beta\, Y_{i\pm1,j} + \gamma\, Y_{i,j\pm1} \\ 1 &= \alpha + \beta + \gamma \end{aligned}$$

Where X_P and Y_P are the coordinates of the point to be localized, P. If the coefficients α, β and γ are less than or equal to one, and are all positive, then the point P lies inside the triangle. If not, the search location $G_{i,j}$ is advanced along the grid lines as shown by arrows and circles in Figure 1. Finally, the triangle into which the point P falls is localized as depicted by the circles at its vertices. Once the point is localized, the coefficients α, β and γ give the geometric interpolation weights at the point P in terms of the function values at the three interpolation points. Thus, interpolation weights are readily available to interpolate flow variables at the point P from the donor grid.

The directional search process with a different starting point is also depicted in figures 1a. The sequential localization of several points is depicted in Figure 1b. As shown, the search process for localizing the next consecutive point starts from the $G_{i,j}$ grid point which localizes the previous point.

In this work, the above localization process is applied to overlapping/overset subgrids moving relative to each other. The boundary point localization and the interpolation of flow variables are performed at every time step as the computational grids move relative to each other in an unsteady motion. The localization process also gives the interpolation weights. Thus, the flow variables at the intergrid boundary points may be interpolated from the donor grid simultaneously. Since the intergrid boundary points are localized sequentially and the localization algorithm is unified with the interpolation scheme, the application of the intergrid boundary conditions becomes quite robust and efficient. It should also be noted that no interpolation data needs to be stored. Flow variables are interpolated across overset grids as an integral part of the localization of intergrid boundary points.

NAVIER–STOKES SOLVER

An implicit, thin–layer, Navier-Stokes solver[8,9,10] with the third order accurate Osher's upwind biased flux difference splitting scheme is employed to compute the flowfield in each computational grid. The strong conservation–law form of the 2–D, thin–layer Navier–Stokes equations in a curvilinear coordinate system, (ξ, ζ), along the axial and normal direction respectively, is given as follows

$$\partial_t \hat{\mathbf{Q}} + \partial_\xi \hat{\mathbf{F}} + \partial_\zeta \hat{\mathbf{G}} = Re^{-1} \partial_\zeta \hat{\mathbf{S}} \qquad (1)$$

Where $\hat{\mathbf{Q}}$ is the vector of conservative variables, $1/J(\rho, \rho u, \rho w, e)$, $\hat{\mathbf{F}}$ and $\hat{\mathbf{G}}$ are the inviscid flux vectors, and $\hat{\mathbf{S}}$ is the thin layer approximation of the viscous fluxes in the ζ direction normal to the airfoil surface:

$$\hat{\mathbf{F}} = \frac{1}{J}\begin{pmatrix} \rho U \\ \rho u U + \xi_x p \\ \rho w U + \xi_z p \\ (e+p)U - \xi_t p \end{pmatrix}, \quad \hat{\mathbf{G}} = \frac{1}{J}\begin{pmatrix} \rho W \\ \rho u W + \zeta_x p \\ \rho w W + \zeta_z p \\ (e+p)W - \zeta_t p \end{pmatrix}$$

$$\hat{\mathbf{S}} = \frac{1}{J}\begin{pmatrix} 0 \\ \mu m_1 u_\zeta + (\mu/3) m_2 \zeta_x \\ \mu m_1 w_\zeta + (\mu/3) m_2 \zeta_z \\ \mu m_1 m_3 + (\mu/3) m_2 + (\zeta_x u + \zeta_z w) \end{pmatrix}$$

where

$$\begin{aligned} m_1 &= \zeta_x^2 + \zeta_z^2 \\ m_2 &= \zeta_x u_\zeta + \zeta_z w_\zeta \\ m_3 &= (u^2 + w^2)/2 + \kappa Pr^{-1}\left(\frac{\partial a^2}{\partial \zeta}\right) \end{aligned}$$

and U, W are the contravariant velocity components. In the above equations, all dimensions are normalized with the airfoil chord length, c. ρ is the density normalized with the free–stream density ρ_∞; u and w are the Cartesian velocity components in the physical domain, which are normalized with the free–stream speed of sound a_∞; e is the total energy per unit volume normalized with $\rho_\infty a_\infty^2$; and Pr is the Prandtl number. The pressure is related to density and total energy through the equation of state for an ideal gas, $p = (\gamma - 1)\left[e - \rho(u^2 + w^2)/2\right]$.

The flowfield is assumed to be fully turbulent. The Baldwin–Lomax algebraic turbulence model and the Baldwin–Barth one equation turbulence model[11,12] are currently implemented. The Baldwin-Barth model gives a continuous turbulent eddy viscosity distribution across the intergrid boundaries and well suited for solutions with overset grids, however it has a time-step limitation for unsteady flowfields.

Boundary Conditions

Boundary conditions are applied on the airfoil surfaces, and at the farfield and intergrid boundaries. On the airfoil surfaces the no–slip boundary condition is applied. For the flapping airfoil, the surface fluid velocity is set equal to the prescribed airfoil flapping velocity so that the no–slip condition is satisfied. Since the formulation of the Navier-Stokes solver is based on an inertial frame of reference, the flapping motion of the airfoil is implemented by moving the airfoil and the computational grid around it in the transverse direction as described by the frequency and the amplitude of the flapping motion. The density and the pressure values on the airfoil surfaces are obtained from the interior by a simple extrapolation.

At the farfield inflow and outflow boundaries the flow variables are evaluated using the zero–order Riemann invariant extrapolation.

At the overlapping/overset intergrid boundaries, the conservative flow variables are interpolated at every time step using the present boundary point localization and interpolation method.

In the Baldwin-Barth turbulence model, the free stream turbulent Reynolds number is set to 0.1. At the intergrid boundaries, turbulent Reynolds number is similarly interpolated from the donor grid.

Numerical Implementation

The numerical integration in each computational grid is performed using an upwind biased, factorized, iterative, implicit, numerical scheme[13] given by

$$
\begin{aligned}
&\left[I + h_\xi \left(\nabla_\xi^b \tilde{A}^+_{i,k} + \Delta_\xi^f \tilde{A}^-_{i,k}\right)\right]^p \\
&\quad \times \left[I + h_\zeta \left(\nabla_\zeta^b \tilde{B}^+_{i,k} + \Delta_\zeta^f \tilde{B}^-_{i,k} - Re^{-1}\delta_\zeta \tilde{M}_{i,k}\right)\right]^p \\
&\quad \times \left(\tilde{Q}^{p+1}_{i,k} - \tilde{Q}^p_{i,k}\right) \qquad (2) \\
= &\quad -\Big[\left(\tilde{Q}^p_{i,k} - Q^n_{i,k}\right) \\
&\quad + h_\xi \left(\hat{F}^p_{i+1/2,k} - \hat{F}^p_{i-1/2,k}\right) \\
&\quad + h_\zeta \left(\hat{G}^p_{i,k+1/2} - \hat{G}^p_{i,k-1/2}\right) - \\
&\quad - Re^{-1} h_\zeta \left(\hat{S}^p_{i,k+1/2} - \hat{S}^p_{i,k-1/2}\right) \Big]
\end{aligned}
$$

In Eq. (8), $h_\xi = \Delta\tau/\Delta\xi$ etc. and $\tilde{A}^\pm = (\partial\tilde{F}/\partial\tilde{Q})$ etc. are the flux Jacobian matrices, and Δ, ∇, and δ are the forward, the backward and the central difference operators, respectively. The quantities $\tilde{F}_{i+1/2,k}$ and $\tilde{G}_{i,k+1/2}$ and $\tilde{S}_{i,k+1/2}$ are numerical fluxes. The superscript ^{n} denotes the time step and ^{p} refers to Newton subiterations within each time step.

The inviscid fluxes $\hat{F}$ and $\hat{G}$ are evaluated using Osher's third–order–accurate upwinding scheme. For the linearization of the left–hand side of Eq. (2) the flux

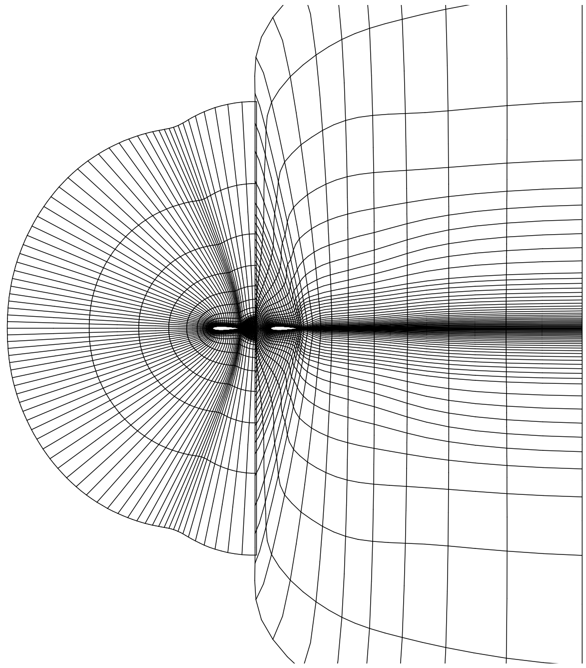

Fig. 2 Overlapping C-grids for an airfoil combination in tandem. (Every other grid point is plotted.)

Jacobian matrices A, B are evaluated by the Steger–Warming flux–vector splitting. The viscous fluxes $\hat{S}$ are computed with second–order–accurate central differences.

The numerical integration at the hole grid points is accommodated by *i-blanking*, which replaces the corresponding coefficient matrices by an identity matrix and sets the right hand side to zero. This process essentially imposes no change in the flow variables on the hole grid points.

In the implementation of the Baldwin-Barth turbulence model, the governing equation for the turbulent Reynolds number is solved with first-order accuracy. The i-blanking at the hole grid points and the intergrid boundary conditions are similarly applied.

RESULTS AND DISCUSSION

In this work, the present intergrid boundary point localization and interpolation method has been applied to a flapping/stationary airfoil combination in tandem with an overlapping grid, and to a single flapping airfoil with an overset grid. The numerical solutions obtained for a single airfoil with overset grids were compared against single grid solutions.

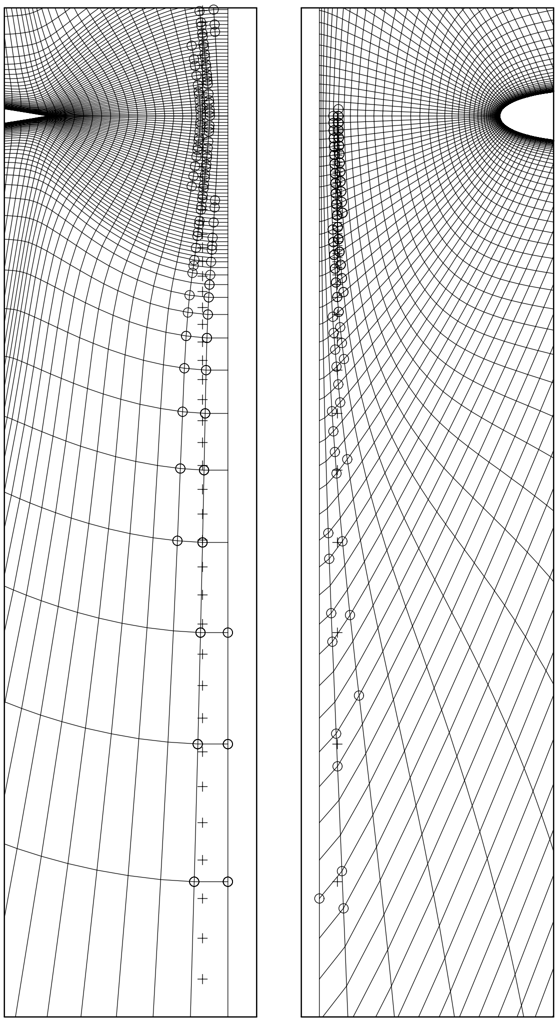

Fig. 3 Localization of intergrid boundary points on overlapping C-grids.

Figure 2 shows the overlapping grid system employed for the solution of the unsteady flowfield over a flapping/stationary NACA0012 airfoil combination in tandem as the leading airfoil undergoes a sinusoidal flapping motion in the cross-flow direction. C-grids around each airfoil are overlapped in the region between the trailing edge of the leading airfoil and the leading edge of the trailing airfoil. The airfoils are placed one chord length distance away from each other and the interface between grids is overlapped by about $0.05c$. As the periodic flapping motion is imposed on the upstream airfoil, the upstream grid moves with respect to the downstream grid in the inertial frame of reference. The overlapping boundary points on each grid are then localized on the donor grid and the flow variables are

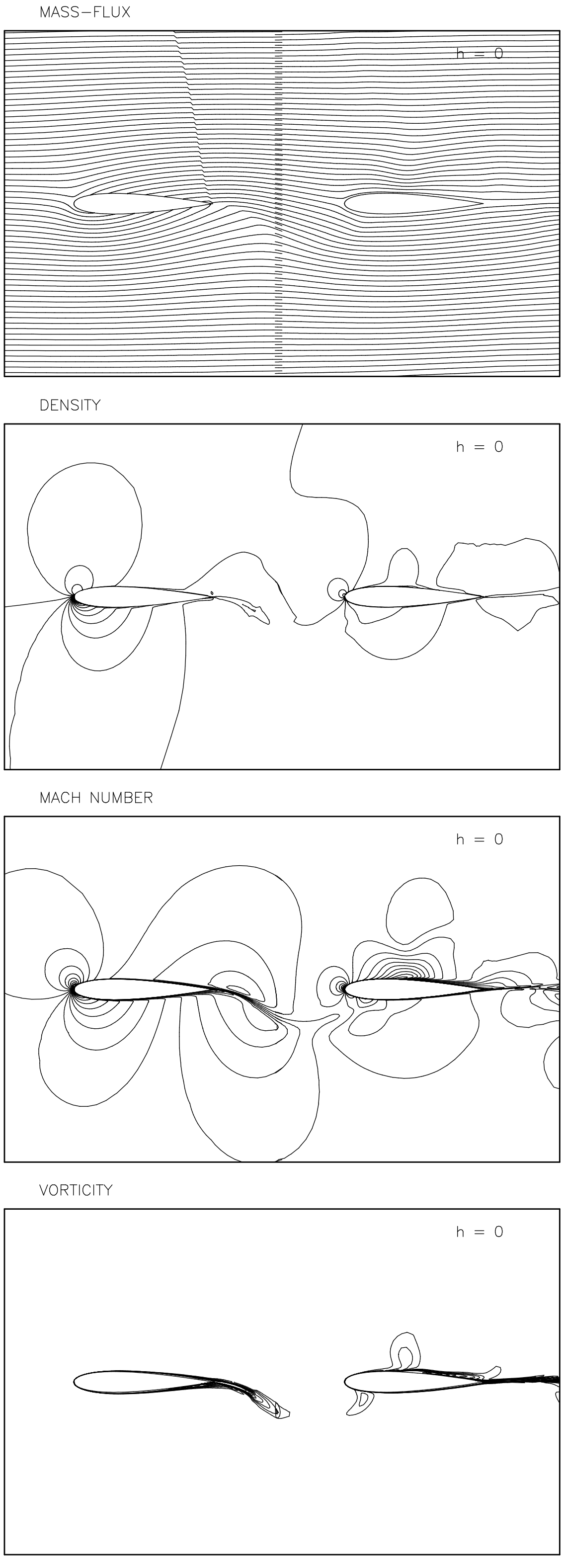

Fig. 4 Instantaneous flowfield computed with the overlapping C-grids - $h = -0.10c\cos(\omega t)$, $\omega c/2U_\infty = 1.5$, $M_\infty = 0.3$, $Re = 3 \cdot 10^6$.

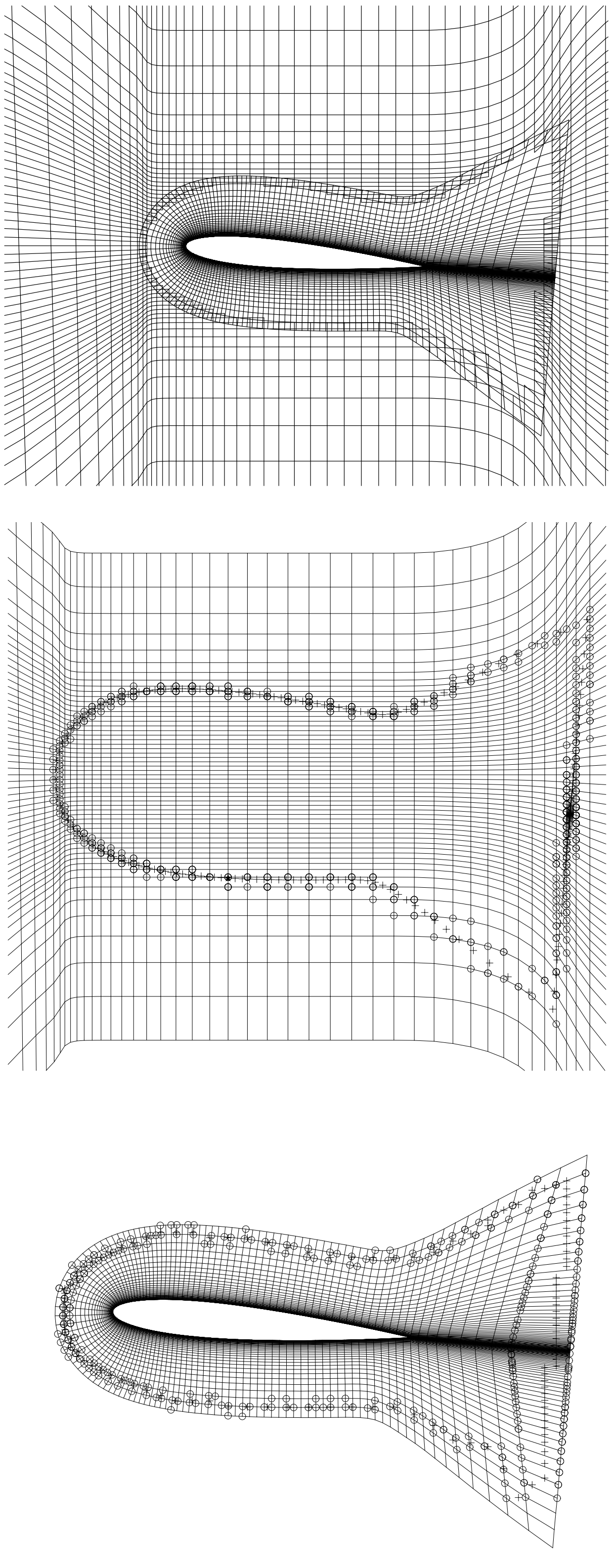

Fig. 5 Overset grid system at $\alpha = 5°$ and localization of the intergrid boundary points.

interpolated simultaneously. The sequential localization of the overlapping boundary points on each grid is partially shown in Figure 3.

The unsteady flowfield is computed at $k = \omega c/2U_\infty = 1.5$, $M_\infty = 0.30$ and $Re = 3\text{x}10^6$. c denotes the chord length. The flapping motion is defined by $h = -0.10c\cos(\omega t)$. The Baldwin-Lomax turbulence model is used in each grid. Figure 4 shows the instantaneous flowfield in terms of mass-flux, density, Mach number and vorticity contours as the leading airfoil passes through its mean position, $h = 0$. The continuity of the contour lines across the overlapping boundaries indicates that the overlapping boundary conditions are applied successfully. An extensive study on the airfoil interference effects, which utilizes the present method, is presented in references 8 and 9.

Next, steady and unsteady flowfields around a single NACA0012 airfoil is computed with overset grids and compared with single grid solutions. In Figure 5, the overset C-grid system and the localization of the intergrid boundary points are shown. A 137×51 size viscous C–grid around the airfoil is overset onto a clustered 71×71 size rectangular base grid at $\alpha = 5°$ incidence. There are 121 grid points around the airfoil and the grid spacing normal to the airfoil surface varies from 2×10^{-5} at the leading edge to 5.5×10^{-5} at the trailing edge. As shown in Figure 5b, the outer boundary points of the overset C–grid, which are denoted by the + sign, are first localized sequentially on the base grid. This process defines the boundary points of the hole cut in the base grid. The overlapping intergrid boundary is then enlarged by extending the boundaries of the hole on the base grid by one grid point inward in both i and j directions. This process ensures that all the boundary points defining the hole fall into the C–grid. An indexing array is utilized to denote the hole points on the base grid. Next, as shown in Figure 5c, the extended boundary points of the hole on the base grid are localized on the overset C–grid.

In Figures 6 and 7, a steady-state flowfield computed at $\alpha = 5°$ on this overset C–grid system is compared to a single C–grid solution. The single C–grid is of 181x81 size and is the extension of the C–grid used in the overset C–grid system. The eddy viscosity field is computed by the Baldwin-Barth one–equation turbulence model in each grid with intergrid boundary conditions. As shown in the figures, the contour lines of the flow variables are continuous across the grid boundaries and in excellent agreement with the single grid solution, which again indicate that the flow variables are accurately interpolated across the intergrid boundaries.

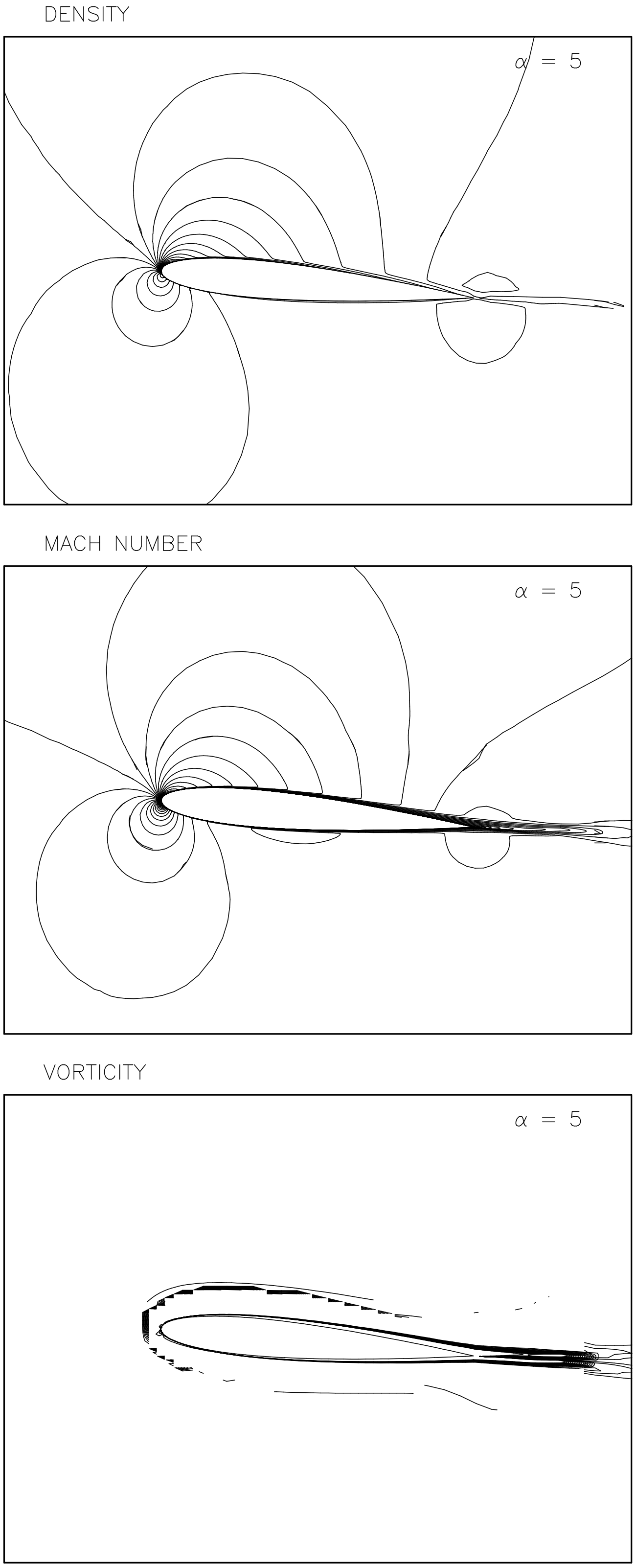

Fig. 6 Flowfield computed on the overset grid - Steady state at $\alpha = 5°$, $Re = 3 \cdot 10^6$, $M_\infty = 0.3$

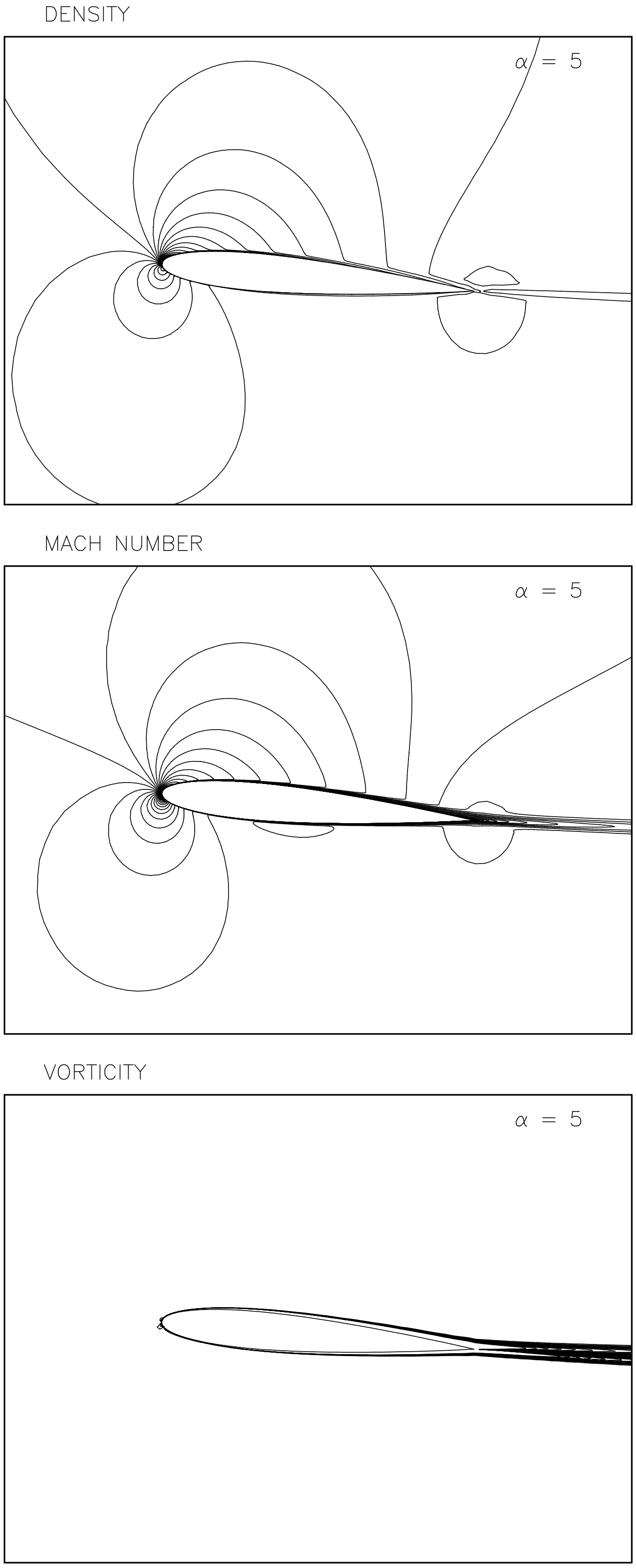

Fig. 7 Flowfield computed on the single grid - Steady state at $\alpha = 5°$, $Re = 3 \cdot 10^6$, $M_\infty = 0.3$

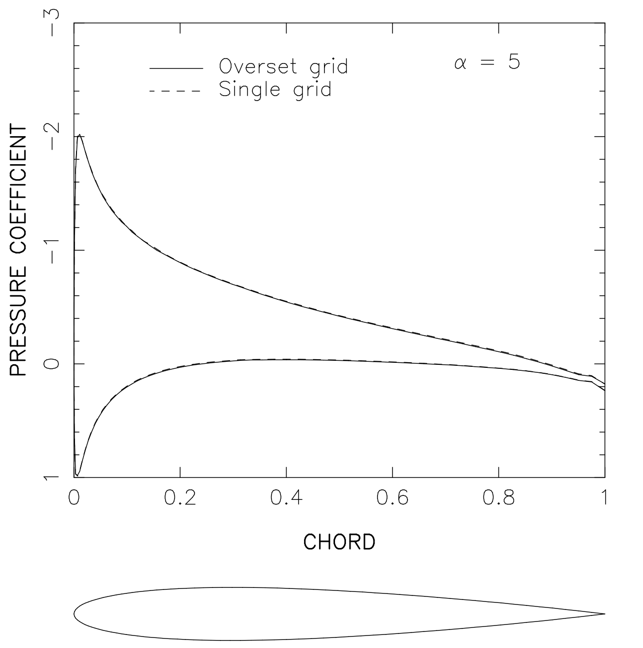

Fig. 8 Surface pressure distribution - Steady state at $\alpha = 5°$, $Re = 3 \cdot 10^6$, $M_\infty = 0.3$

However, it is also noted that the interpolation of the flow variables from the highly clustered overset C–grid at the downstream end of the wake cut onto the coarser base grid dissipates the vorticity in the wake. Figure 8 shows the excellent comparison of surface pressures.

Next, the same overset C grid is employed for an unsteady solution as the airfoil, which is now set at $\alpha = 0°$, undergoes a periodic flapping motion. The flapping motion is defined by $h = -0.10c\cos(\omega t)$ at a reduced frequency of $\omega c/2U_\infty = 0.5$. The intergrid boundary conditions are applied at every time step as the overset C–grid moves in the cross-flow direction relative to the base grid. In this unsteady computations, the Baldwin-Lomax algebraic eddy viscosity model was employed only on the viscous C-grid. The Baldwin-Barth model had convergence problems at this relatively high frequency motion and corrupted the solution. In Figures 9 and 10 the instantaneous flowfield as the airfoil passes the $h = 0$ position with the maximum velocity is compared against the single grid solution. The computed flowfields are again in excellent agreement. The comparison of unsteady aerodynamic loads is also given in Figure 11. Note that the flapping motion generates thrust[8,9]. The unsteady overset grid solution at this relatively high frequency flapping motion again

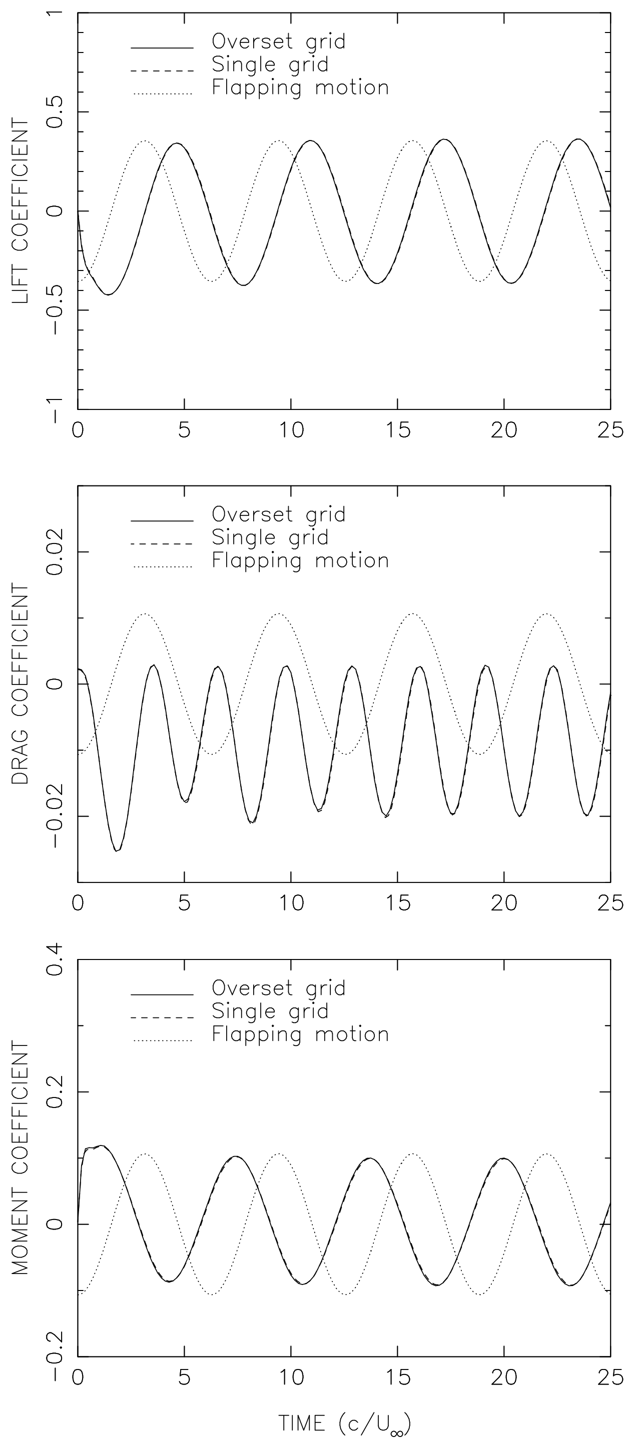

Fig. 11 Time history of the unsteady aerodynamic loads - Flapping airfoil with $h = -0.10c\cos(\omega t)$, $\omega c/2U_\infty = 0.5$, $M_\infty = 0.3$, $Re = 3 \cdot 10^6$.

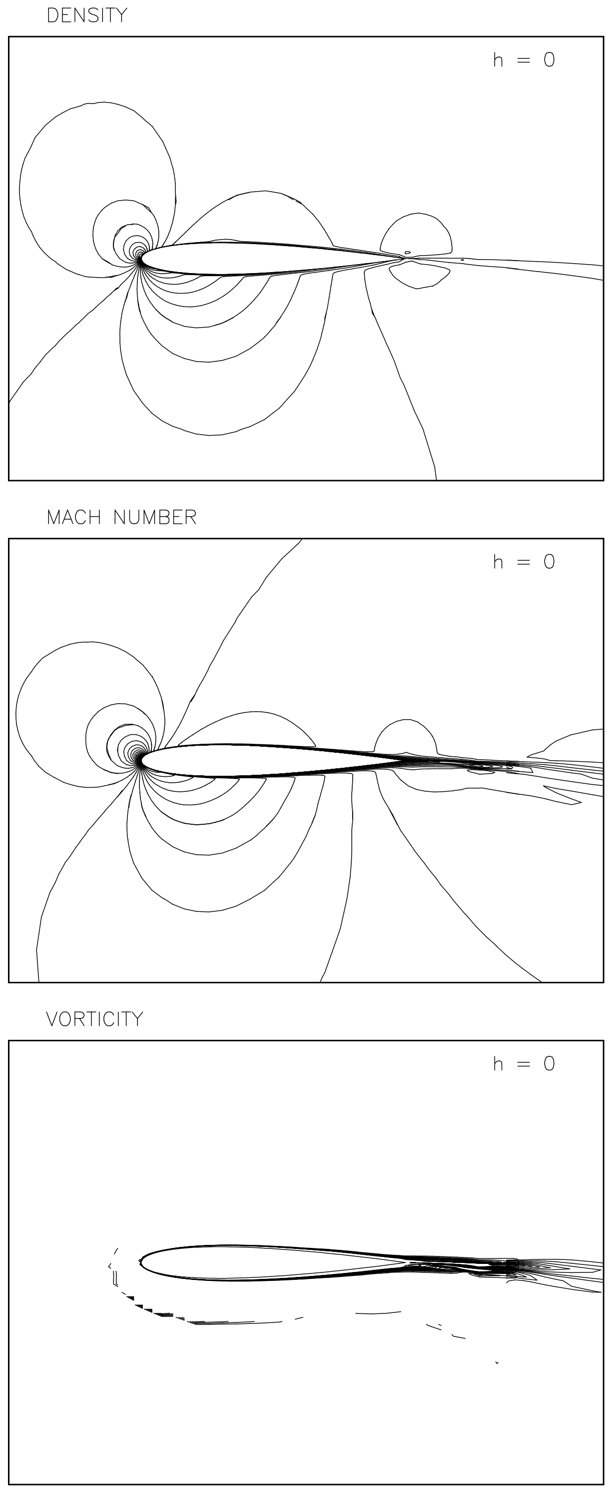

Fig. 9 Instantaneous flowfield computed on the overset grid at $tU_\infty/c = 14.10, h = 0.0$ - Flapping NACA0012 airfoil with $h = -0.10c\cos(\omega t)$, $\omega c/2U_\infty = 0.5$, $M_\infty = 0.3$, $Re = 3 \cdot 10^6$.

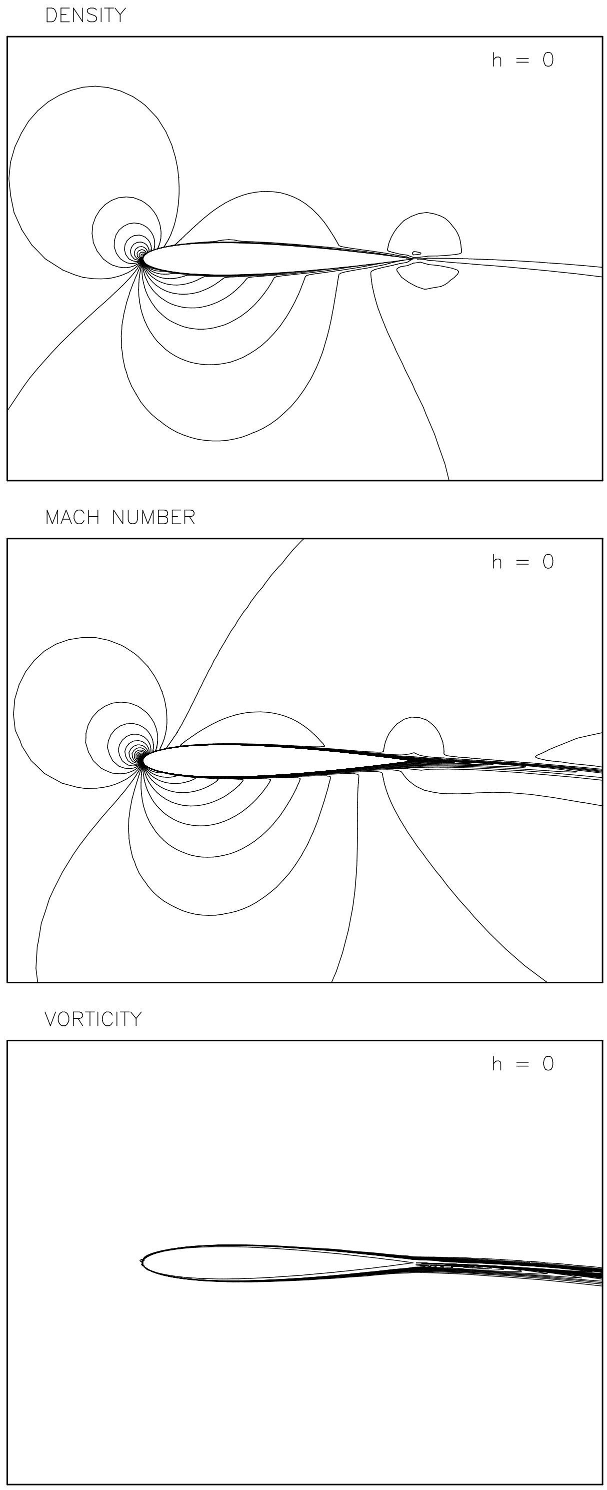

Fig. 10 Instantaneous flowfield computed on the single grid at $tU_\infty/c = 14.10, h = 0.0$ - Flapping NACA0012 airfoil with $h = -0.10c\cos(\omega t)$, $\omega c/2U_\infty = 0.5$, $M_\infty = 0.3$, $Re = 3 \cdot 10^6$.

agrees remarkably well with the single grid solution.

CONCLUDING REMARKS

A new method for the solution of unsteady Navier-Stokes equations on overlapping/overset grids is presented. In this method, intergrid boundary points are localized by a directional search algorithm and flow variables across the grids are interpolated as an integral part of the boundary point localization process in the main solver. No external interpolation data is stored. Steady and unsteady flowfield solutions were found to be in excellent agreement with the single grid solutions. The application of the intergrid boundary conditions with the present boundary point localization and interpolation method is, therefore, highly accurate and robust. It should also be noted that the present method is independent of numerical solution algorithms. It may easily be implemented on any 2-D, single block flow solver to make it a multi-block, zonal solver regardless of the solution algorithm and the flow variables employed.

REFERENCES

1. Thompson, J.F. and Weatherill, N.P, August 1993, *Aspects of Numerical Grid Generation: Current Science and Art,* AIAA Paper 93-3539-CP, Applied Aerodynamics Conference.

2. Steinbrenner, J.P., Chawner, J.R. and Fouts, C.L., 1990, *Multiple Block Grid Generation in the Interactive Environment.*, AIAA Paper 90–1602.

3. Thompson, J.F. 1988, *Composite Grid Generation Code for General 3-D Regions – the EAGLE Code,*, AIAA Journal, 26.3: 271-272.

4. Barth, J.T., May 1992, *Aspects of Unstructured Grids and Finite–Volume Solvers for Euler and Navier–Stokes Equations,* AGARD Report 787, Special course notes.

5. Mavripilis, D., 1988, *Adaptive Mesh Generation for Viscous Flows Using Delaunay Triangulation,*, ICASE Repost No. 88-47.

6. Morgan, K, Perarie, J. and Perio, J., May 1992, *Unstructured Grid Methods for Compressible Flows,* AGARD Report 787, Special course notes.

7. Benek, J.A., Buning P.G. and Steger J.L., 1985, *A 3-D Chimera Grid Embedding Technique*, AIAA paper 85–1523.

8. Tuncer, I.H. and Platzer, M.F., *Thrust Generation due to Airfoil Flapping,* to be published in the AIAA Journal.

9. Tuncer, I.H and Platzer, M.F., *Analysis of Unsteady Airfoil Interference Effects Using a Zonal Navier-Stokes Solver*, AIAA paper 95–0307.

10. Tuncer, I.H, Ekaterinaris, J.A. and Platzer, M.F., *A Viscous-Inviscid Interaction Method for Unsteady Low Speed Airfoil Flows,* I.H. Tuncer, J.A. Ekaterinaris and M.F. Platzer, AIAA Journal, Vol. 33, No. 1, January 1995, pp. 151-154.

11. Baldwin, B.S. and Barth, T.J., *A One-Equation Turbulence Transport Model for High Reynolds Number Wall-Bounded Flows,* NASA TM 102847, 1990.

12. Barth, T.J., *Private communications,* 1995.

13. Rai, M. M. and Chakravarthy, S. R., *An Implicit Form of the Osher Upwind Scheme,* AIAA Journal, Vol. 24, No. 5, May 1986, pp. 735–743.